S. Pandini, F. Bignotti, F. Baldi, L. Sartore, G. Consolati, G. Panzarasa
Thermomechanical and Large Deformation Behaviors of Antiplasticized Epoxy Resins: Effect of Material Formulation and Network Architecture
Polymer Engineering and Science, Vol. 57, N. 6, 2017, p. 553-565
doi:10.1002/pen.24555

Thermomechanical and Large Deformation Behaviors of Antiplasticized Epoxy Resins: Effect of Material Formulation and Network Architecture

Stefano Pandini,[1] Fabio Bignotti,[1] Francesco Baldi,[1] Luciana Sartore,[1] Giovanni Consolati,[2] Guido Panzarasa[3]

[1] *Department of Mechanical and Industrial Engineering, University of Brescia, Via Branze 38, Brescia 25123, Italy*

[2] *Department of Aerospace Science and Technology, Politecnico di Milano, Piazza Leonardo da Vinci 32, Milano 20133, Italy*

[3] *Department of Polymer Engineering and Science, Montanuniversität, Otto-Glöckel Strasse 2, Leoben 8700, Austria*

A series of amine-hardened epoxies were prepared by systematically varying the stoichiometric ratio and the relative amounts of diepoxide and monoepoxide resin to chemically control the material composition and macromolecular architecture (chain segments flexibility; cross-link density; amounts of dangling groups). Positron Annihilation Lifetime Spectroscopy was used to investigate the free volume associated to the various epoxy formulations, while dynamic-mechanical analysis was employed to investigate their network density and their primary and secondary mechanical relaxations. The mechanical behavior at small and large strain was studied by means of tensile and compression tests. The results pointed out that deviations from the ideal stoichiometric composition and the addition of monoepoxide resins lead to significant room temperature stiffening, together with a reduction of the cross-link density and glass transition temperature. This behavior, phenomenologically associated to antiplasticization, was interpreted according to the specific macromolecular architecture and ascribed to chain mobility hindrance, as revealed by secondary transitions, whereas no significant contribution from the free volume could be evidenced. Furthermore, it was shown that depending on the strain scale and on the corresponding deformational mechanisms, the mechanical response may be differently influenced either by the presence of dangling groups or by the network density. POLYM. ENG. SCI., 00:000–000, 2017.

INTRODUCTION

Epoxy resins are a large class of thermosetting polymers that encounter large interest in various technological applications (e.g., adhesives, coatings and high-performance composites) thanks to their thermomechanical and chemical properties and to the possibility to tailor their performances on the basis of the specific chemical compounds employed in the resin formulations.

Epoxy resins are usually prepared through cross-linking of epoxy oligomers with active-hydrogen compounds, such as anhydrides and aromatic or aliphatic polyamines, termed as hardeners. A proper formulation of the reaction mixture, through the variation of as the stoichiometric ratio [1–10], the type of resin and hardener [2, 11–13], the use of chains extenders [13] or blends of different monomers [7, 8, 15], allows to significantly vary the chemical and physical properties of the resins. In particular, their mechanical response at small and large strains [15], their thermomechanical behavior [2], and their fracture resistance [17–20] may be significantly influenced by parameters related to the specific resin formulation, such as the choice of specific hardener-to-resin ratios, which is perhaps the easiest way to vary the mechanical response of epoxy resins and epoxy-based particulate composites [1, 6–8, 20, 21].

Under specific formulations, epoxy resins may exhibit a peculiar mechanical effect, called "internal antiplasticization," which consists in the simultaneous occurrence of the following phenomena: (1) a reduction of T_g (usually promoted by the incorporation of plasticizers or by the reduction of the cross-link density); (2) a room temperature stiffening (typically consisting of an increase of the room temperature tensile modulus and strength); and (3) a reduction of the impact strength and elongation at break. This behavior is found also in uncross-linked polymers, where it is typically associated to the presence of low-molecular-weight additives (called antiplasticizers or fortifiers), which exert a local hindrance to chain mobility on temperature regions below the glass transition temperature [22–25]. In epoxy resins, antiplasticization has been observed mostly in nostoichiometric or partially reacted systems [16], or when using monoamine chain extenders [16, 26], and interpreted as the effect of unreacted molecules or dangling chains (antiplasticizing groups) able to induce an alteration of the secondary relaxation processes.

Antiplasticization seems also to affect the response at large strain (i.e., yield and postyield), revealing an even more complex dependence of the resin response on parameters, such as chain flexibility [14, 15], relaxation behavior (i.e., glass transition [11, 12]) and material structure (e.g., the cross-link density [27]). In epoxy resins, yield strength is mainly governed by the molecular mobility. In systems with varied formulation, it may be influenced both by the reduction of segmental mobility due to the presence of antiplasticizers, [23, 28] and by the change in cross-link density [14, 29]. Interestingly, Rana et al. [30], by investigating the dependence of yield stress on temperature and on antiplasticizers content, have shown that both antiplasticization-related β-type relaxation and network-related α-type relaxation may concur in determining the material

Correspondence to: S. Pandini; email: stefano.pandini@unibs.it
First presented as poster at TOP Conference 2016—8th International Conference on Times of Polymers and Composites, June 19–23, 2016, Ischia, Italy.
DOI 10.1002/pen.24555
Published online in Wiley Online Library (wileyonlinelibrary.com).

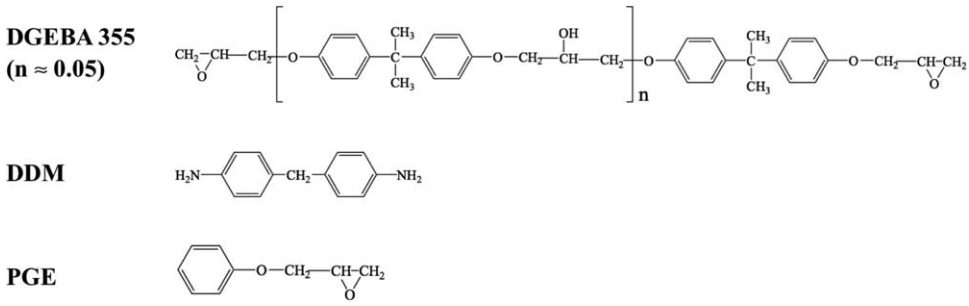

FIG. 1. Chemical structure of the monomers employed in the preparation of the epoxy resins.

resistance to yielding. In contrast, the postyield strain softening and hardening behavior is seen to be mainly ruled by the cross-link density [27], and a further contribution may be provided by physical cross-linking, as that ascribed to hydrogen bonding between the network segments and the antiplasticizers [31]. It is anyway important to remark that in presence of complex formulations, such as those achieved by changing the resin/hardener ratio, where segmental chain mobility and cross-link density are simultaneously varied, the behavior at yield and postyield is governed by a combination of these effects which cannot be separated [6].

Furthermore, one of the current interpretations of antiplasticization calls for a reduction in the free volume of the polymer [32–34]. Positron annihilation lifetime spectroscopy (PALS) is an experimental technique allowing the accurate investigation of free volume for a variety of polymers [35] and has been widely applied to epoxy resins to study the effect of formulation [36], curing [37] and presence of fillers [38] on free volume, in order to explain their mechanical properties [39, 40] and molecular diffusion phenomena [41]. This technique is based on the fact that a fraction of positrons injected in the material may generate positronium (Ps), an unstable bound electron-positron system which gets trapped in the sub-nanometric holes forming the free volume [42], and undergoes annihilation by interacting with one of the electrons belonging to the cavity in a relative singlet state. As a consequence, by measuring its lifetime, it is possible to estimate the size of the free volume holes. Since the results found in the literature are quite dependent on the formulation, PALS measurements would be a helpful technique in order to shed light on the role of the free volume on antiplasticized systems.

The aim of this work is to evaluate the change in the mechanical and thermal properties of antiplasticized amine-hardened epoxy resins, so to better understand the capabilities of tailoring approaches based on the formulation of the reaction mixture. Furthermore, while in most of the literature, the effects of antiplasticization are described by focusing either the small or large strain properties, in the present paper, the effects of antiplasticization are investigated on the whole strain regime. To this purpose, a series of structurally related epoxy resins were prepared, according to two families of systems: one represented by off-stoichiometry systems, obtained by mixing various amounts of epoxy resin (DGEBA 355) and a diamine hardener (diaminodiphenylmethane; DDM), leading to a simultaneous variation of the chemical composition and the cross-link density; the other obtained by adding various amounts of a monofunctional epoxide (phenyl glycidyl ether; PGE) to the epoxy resin and hardener mixture, thus changing the cross-link density with only minor effect on composition. The systems prepared were characterized with the aid of different techniques. Positron annihilation lifetime spectroscopy was used to investigate changes in free volume contents in the various resins, while differential scanning calorimetry (DSC) tests and dynamic-mechanical thermal analysis (DMTA) allowed to determine the thermomechanical features of the various systems. Eventually, uniaxial tensile and compression tests were used to evaluate the small and large strain behavior of the different systems.

EXPERIMENTAL

Materials

Resin DGEBA 355, 4-4′-diaminodiphenylmethane (DDM), and phenyl glycidyl ether (PGE) were purchased from Sigma-Aldrich Co. (Saint Louis, USA) and used without purification.

The equivalent mass values of DGEBA 355, DDM, and PGE were assumed to be 177.5, 49.6, and 150.2 g/eq, respectively. The chemical structure of the three reactants is represented in Fig. 1.

Resins Preparation

The epoxy resins were prepared with different formulations, easily identified through the stoichiometric ratio, q, and the PGE fraction, f_{PGE}, defined as follows:

$$q = \frac{eq_{EP}}{eq_{AM}} \tag{1}$$

$$f_{PGE} = \frac{eq_{EP1}}{eq_{EP1} + eq_{EP2}} = \frac{eq_{EP1}}{eq_{EP}} \tag{2}$$

where eq_{EP1} is the number of epoxy equivalents (i.e., moles of epoxy groups) from the monofunctional epoxy component (PGE), eq_{EP2} is the number of epoxy equivalents from the difunctional epoxy component (DGEBA 355), eq_{EP} is the total number of epoxy equivalents, and eq_{AM} is the number of amine equivalents (i.e., the moles of amine hydrogens) in the starting reaction mixture. In the following, the resins obtained from DGEBA 355 and DDM (without PGE) will be identified by the code EP-q−0, while the ternary systems will be coded as EP-q-f_{PGE}.

A list of the materials investigated, along with the corresponding codes, is reported in Table 1.

 DOI 10.1002/pen

TABLE 1. Glass transition temperature of the mixtures cross-linked in the DSC ($T_{g,mixture}$), employed to designate the initial and final temperatures for the specimen curing cycle ($T_{cure,in}$ and $T_{cure,fin}$, respectively).

Material code	q	f_{PGE}	$T_{g,mixture}$ (°C)	$T_{cure,in}$ (°C)	$T_{cure,fin}$ (°C)
EP-0.7-0	0.70	0	135	115	155
EP-0.9-0	0.90	0	170	130	190
EP-1.0-0	1.00	0	178	135	200
EP-1.1-0	1.10	0	148	120	170
EP-1.3-0	1.30	0	110	100	130
EP-1.0-0.10	1.0	0.1	151	120	170
EP-1.0-0.20	1.0	0.2	132	110	150
EP-1.0-0.30	1.0	0.3	115	100	135
EP-1.0-0.50	1.0	0.5	87	90	110
EP-0.7-0.30	0.70	0.3	84	100	100
EP-0.9-0.30	0.90	0.3	106	100	130
EP-1.1-0.30	1.10	0.3	103	95	125
EP-1.3-0.30	1.30	0.3	61	100	100

Preliminary DSC curing experiments were carried out for the various compositions, in order to measure the glass transition temperature of the fully cross-linked mixture ($T_{g,mixture}$) and the temperatures at which the specimens to be employed in mechanical tests had to be oven-cured to ensure full cross-linking of the various compositions ($T_{cure,in}$ and $T_{cure,fin}$; see Table 1). More precisely, $T_{cure,in}$ was set as the average value between 90°C and $T_{g,mixture}$, while $T_{cure,fin}$ was chosen as $T_{g,mixture}$ + 20°C.

The epoxy components (either DGEBA 355 for series EP-q−0 or the proper combination of DGEBA 355 and PGE for series EP-q-f_{PGE}) and the hardener were mixed under stirring at 50°C. The resulting mixture was degassed under vacuum, poured into silicone molds, which were preheated at 90°C, and heated in an oven at the initial cure temperature, $T_{cure,in}$. After 18–20 h at $T_{cure,in}$, the material was heated at the final cure temperature, $T_{cure,fin}$, to complete the cross-linking process, and subsequently slowly cooled to room temperature.

The specimens were prepared, by casting the resin in silicon moulds, according to two geometries: (1) rectangular specimens (length = 90 mm; width = 7 mm; thickness = 1 and 2 mm), employed for the tensile test measurements and for the dynamic mechanical characterization, and (2) cylindrical specimens (height = 10 mm; diameter = 7.5 mm), employed in the large deformation measurements under compression.

DSC Tests

DSC experiments were carried out by heating the samples in aluminum crucibles in a differential scanning calorimeter DSC1 Star system by Mettler Toledo (Columbus, OH, USA), under a nitrogen flow of 70 mL/min.

The preliminary DSC cure experiments were run by first heating about 15 mg of the monomer mixture from 50 to 260°C at 5°C/min, later cooling the cross-linked system to 50°C at 10°C/min and finally reheating to 260°C at 10°C/min to evaluate the presence of any residual uncross-linked resin fraction and determine $T_{g,mixture}$, the T_g of the fully cross-linked mixture.

The DSC experiments on cured specimens were carried out on thin slices of about 5 mg, cut from the central portion of the rectangular bars. The samples were first heated from 30 to 20°C above their T_g at 10°C/min, maintained at that temperature for 1 min, cooled down to 30°C at 10°C/min and reheated up to 220°C at 10°C/min. The glass transition temperature of the cured resin was taken in correspondence of the inflection point in the second heating scan trace.

DMTA Tests

The materials were subjected to dynamic mechanical thermal analysis (DMTA), by means of a DMA Q800 (TA Instrument). The tests were carried out under a tensile configuration on bar-shaped specimens (average gauge length: 18 mm; width ≈ 7 mm; thickness ≈ 1 mm), under the application of a displacement amplitude of 15 μm and at a frequency of 1 Hz. All the samples were subjected to a heating ramp at 1°C/min on a range between room temperature (i.e., at least 70°C below T_g) and a temperature at least 40°C above the glass transition temperature, with the aim to properly evaluate the temperature of the principal glass transition and the storage modulus in the rubber-like plateau, E'_r. An estimation of the cross-link density, ν, defined as the concentration of effective elastic chains, was carried out on rubber-like storage modulus according to the classical theory of rubber elasticity through the following equation [43]:

$$E'_r = 3ART\nu \tag{3}$$

where R is the gas constant, T is the absolute temperature, and A is the so-called front factor, whose value should be unity for networks undergoing affine deformation. The value of E'_r was taken 10°C above the temperature where the storage modulus displays its minimum value at the end of the glass transition process, ensuring its evaluation being carried out within the rubber-like plateau.

On some of the investigated systems, the DMTA tests were carried out also on a large temperature interval, ranging from −100°C up to the rubbery plateau region, under the same conditions reported above, with the aim to properly describe both their primary and secondary relaxation processes within the same temperature scan.

Positron Annihilation Lifetime Spectroscopy (PALS)

The positron source, ^{22}Na from a carrier free neutral solution, was deposited between two identical 7.5 μm ®Kapton foils (in which positronium is not formed [44]), glued together and inserted in the specimen to be studied in the usual sandwich configuration. Care was taken to prevent the glue from reaching the region involved in annihilation. Two identical samples in the form of square slabs (1 × 1 cm^2) completely surrounded the source; the thickness of each sample was sufficient to stop the injected positrons. Lifetime spectra were obtained by means of a fast–fast coincidence system; a pair of cylindrical plastic scintillators (NE111 24 × 24 mm) were coupled to photomultipliers Philips XP2020Q. The resolution of the spectrometer was about 290 ps. Each spectrum contained about 8 × 10^6 counts; at least two spectra for each sample were obtained. The fraction of the positrons annihilating in the Kapton was estimated to be about 12%; after subtraction of this contribution the spectra were analyzed by means of the LT program [45]. A three components fit was adopted, consisting in two discrete lifetimes and a continuous distribution (corresponding to positronium decay). The

goodness of the fit, as quantified by normalized chi-square test, was found in every case to be acceptable, being in the range 0.97–1.08.

Tensile Tests

The tensile properties of the resins were measured on bar-shaped specimens, with the employ of an electromechanical dynamometer (Instron, Mod. 3366), equipped with a load cell with a capacity of 10 kN. The specimens (gauge length: 60 mm; width $\approx$ 7 mm; thickness $\approx$ 2 mm) were tested at room temperature until failure, subjecting them to a tensile ramp under displacement control at a displacement rate of 2 mm/min. Three specimens were tested for each system under analysis, abrading them with sandpaper before testing, to uniform their cross section, occasionally uneven due to cross-linking shrinkage, and to avoid local imperfections that may lead to premature failure. The strain was measured by means of a clip-on extensometer in the first part of the tensile ramp (strain up to 0.007) to provide an optimum evaluation of the tensile modulus, after which the extensometer was removed and the elongation was evaluated directly from the crosshead displacement, concurrently recorded.

The values of stress, σ, and strain, ε, were calculated as nominal (or engineering) values, according to the following equations:

$$\sigma = \frac{F}{A_0} \tag{4}$$

$$\varepsilon = \frac{\Delta l}{l_0} \tag{5}$$

where F is the load, A_0 js the initial specimen cross section, Δl is the displacement (measured either by the extensometer or by the dynamometer crosshead) and l_0 is the gauge length (either of the extensometer or of the specimen).

By testing specimens with large length to width ratio, so to minimize the gripping effects on the measured quantities, and by employing an extensometer, it was possible to provide a proper evaluation of both the elastic modulus, and of the stress *versus* strain correlation up to specimen break.

Compression Tests

The large deformation behavior of the resins was investigated in compression tests by means of the electromechanical dynamometer (Instron Mod. 3366). The tests were carried out on cylindrical samples (average diameter: about 7.6 mm; average height: about 9.8 mm), whose faces were abraded with sandpaper to ensure adequately flat and parallel faces at the extremities. The compression plate surfaces were lubricated with paraffin oil before each test in order to reduce the friction between the specimens and the plates.

The tests were carried out under displacement control, at a fixed displacement rate equal to 0.5 mm/min, and were taken beyond the yield stress of the material and up to the maximum load that may be applied (9 kN).

The results are reported in terms of true compressive stress, $\sigma_{t,c}$ (evaluated using the assumption of incompressible deformation) and true compressive strain, $\varepsilon_{t,c}$, which were calculated on the measured values of force and displacement, as follows:

$$\sigma_{t,c} = \frac{F}{A_0} \cdot \left(1 + \frac{\Delta l}{l_0}\right) \tag{6}$$

$$\varepsilon_{t,c} = -\ln\left(1 + \frac{\Delta l}{l_0}\right) \tag{7}$$

where F is the load, A_0 is the initial specimen cross section, Δl is the displacement measured by the dynamometer crosshead, and l_0 is the initial specimen height; the minus sign is reported in order to represent as positive values the compressive stress and strain, since in the formulas, both F and Δl are conventionally taken as negative. The compressive strain was preliminarily corrected by an offset value, so that a zero value of displacement could correspond to the zero load conditions.

Finally, the strain hardening modulus was determined, according to previous studies [28] in which the material was assumed to have in this region a behavior similar to that of a rubbery material (i.e., neo-Hookean behavior): by representing the compressive stress as a function of $-(\lambda^2 - 1/\lambda)$, where $\lambda = (1 + \Delta l/l_0)$, from the correlation

$$\sigma_{t,c} = -G_{SH}\left(\lambda^2 - \frac{1}{\lambda}\right) \tag{8}$$

the strain hardening modulus, G_{SH}, was evaluated as the slope of the final portion of the curve, approximately on a range of strain between 0.8 ε_{max} and ε_{max}, ε_{max} being the maximum strain approached for each curve.

RESULTS AND DISCUSSION

Effect of Formulation on Molecular Architecture and Free Volume Distribution

The epoxy resins were prepared with various compositions to provide a controlled variation of the macromolecular architecture. A first set of materials (systems EP-$q-0$) was prepared by adopting off-stoichiometry formulations, obtained by changing the relative amounts of DGEBA 355 and DDM. This approach provided a simultaneous change of both the cross-link density and the chemical composition, so that it is difficult to distinguish the effect of these two parameters on the material response. For this reason, a second set of materials was prepared with the aim to vary only the cross-link density while providing a minimal composition variation. These systems (systems EP-q-f_{PGE}) were obtained by reacting DDM with a mixture of the difunctional epoxide (DGEBA 355) and the monofunctional epoxide (PGE), while keeping constant the hardener content. Finally, a third set of materials (systems EP-$q-0.30$) were prepared by reacting various amounts of DDM with a mixture of DGEBA 355 and fixed amount of PGE (f_{PGE} = 0.3), so to explore the material response under a hybrid combination of the three ingredients.

The combinations of the three types of ingredients lead to important modifications to the resulting network structure. Although a precise description of the network architecture of cured epoxies is prohibited, due to the possible occurrence of side reactions (e.g., etherification, cyclization, homopolymerization of epoxy resin, and polymer degradation [46]), some qualitative considerations about the expected network architecture can be done, as attempted, for similar systems in ref. 7. According to the theory on stepwise polymerizations [16], under the

 DOI 10.1002/pen

TABLE 2. Results of the DSC and DMTA characterization.

Material code	E'_r (MPa)	ν (mol/m^3)	T_g by DSC (°C)	T_g by DMTA (°C)
EP-0.7-0	19.9	1760	137	141
EP-0.9-0	37.6	3110	168	179
EP-1.0-0	46.9	3790	180	186
EP-1.1-0	28.7	2480	149	153
EP-1.3-0	10.7	1000	107	107
EP-1.0-0.10	29.4	2490	154	164
EP-1.0-0.20	17.9	1580	137	141
EP-1.0-0.30	12.8	1190	116	117
EP-1.0-0.50	2.3	240	87	87
EP-0.7-0.30	2.1	190	86	89
EP-0.9-0.30	9.1	850	110	110
EP-1.1-0.30	13.2	1210	107	117
EP-1.3-0.30	4.9	460	77	81

assumptions of full conversion and absence of side reactions, binary systems at the stoichiometric composition ($q = 1$) would present a closed architecture. With an excess of either amine hydrogens ($q < 1$) or epoxy groups ($q > 1$), a more and more open architecture is expected as the content of the excess component increases, due to the presence of dangling chains and unreacted functions. The incorporation of PGE into the reaction mixture should introduce side chains, in the network structure, deriving from the unreacted moiety of the monofunctional epoxy monomer. Finally, the presence of an excess of either functional group in presence of both mono- and difunctional groups should lead to a hybrid structural configuration with respect to those previously described.

The network cross-link density, ν, was evaluated through *Eq. 3* from the values of storage modulus in the rubber-like plateau, E'_r. The results are reported in Table 2 and in Fig. 2.

By changing the formulation, an overall variation of the cross-link density of about one order of magnitude is achieved, and the use of PGE as network modifier seems to be more effective in changing the cross-link density. In the EP-$q-0$ series, the highest cross-link density is found for the stoichiometric composition ($q = 1$) and decreases as q deviates from unity, while for the EP-1.0-f_{PGE} resins it decreases regularly as the PGE content increases; the same decreasing dependence was observed for all the stoichiometric ratios, q. These results are in agreement with the considerations reported above and with the predictions of the stepwise polymerizations theory.

The investigation of the free volume for the various systems was carried out through positron annihilation lifetime spectroscopy (PALS). Lifetime of ortho-Ps (o-Ps, i.e., the ground state sublevel of positron with parallel spins) is mainly determined by annihilation with the electrons belonging to the cavity where Ps is trapped. Its lifetime is mainly determined by the annihilations of the positron with one of such "external" electrons in a relative singlet state [47]. This involves a correlation between o-Ps lifetime and the sizes of the cavity, which can be cast in a quantitative form by suitably modeling the trapping site [47] and allows to estimate the size of the free volume holes by measuring the o-Ps lifetime.

Various components are associated with the whole positrons lifetime: the shortest lifetime component, attributed to positrons annihilated in the bulk as well as to para-Ps annihilations; the intermediate component, originating from positrons annihilated into defects and free volume holes, their higher lifetime stemming from the fact that the electron density surrounding the positron is lower than that of the bulk; the longest component, which, according to the common interpretation, is ascribed to o-Ps decay. Since we are mainly interested in the lifetime of o-Ps, our discussion will be limited to this latter component.

The relationship between o-Ps lifetime, τ_3, and radius of the free volume hole, R (in spherical approximation), is given by the Tao–Eldrup equation [48, 49]:

$$\tau_3 = \tau_0 \left[\frac{\Delta R}{R+\Delta R} + \frac{1}{2}\sin\left(2\pi \frac{\Delta R}{R+\Delta R}\right) \right]^{-1} \quad (9)$$

where τ_0 is the o-Ps lifetime in the presence of a high electron density and is assumed to be equal to 0.5 ns, and ΔR is an empirical parameter which describes the penetration of the Ps wave function into the bulk, assumed to be equal to 0.166 nm [50]. Furthermore, holes show a distribution of sizes, due to the disordered character of the amorphous zone. This involves a distribution of o-Ps lifetimes, which is supplied from the analysis of annihilation lifetime spectra.

By using a simple mathematical treatment on the distribution of lifetimes [51], the probability density functions of the holes' size distribution have been calculated for the investigated epoxy systems, and are represented in Fig. 3a, for different values of q, and in Fig. 3b, for various PGE contents.

The holes' size distributions are centered at around 0.29 nm, in good agreement with the results reported for a similar system by Goyanes et al. [52] Only the first sample of the q series displays a slightly lower radius (0.2 nm), but this difference is not statistically meaningful by taking into account the experimental uncertainties on the centroids (4.2%). This means that, in spite of the great variation in cross-link density and in the amounts of dangling chains, the average hole size is not affected by either q or f_{PGE}. A comparison between our findings and literature results is not straightforward due to the great variability of epoxy formulations (which does not allow to separate the effect

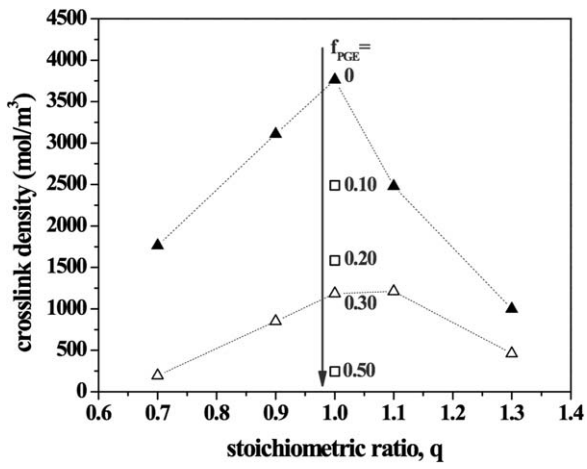

FIG. 2. Cross-link density as a function of the material composition (▲: systems EP-$q-0$, obtained by varying q in the absence of PGE; □: systems EP-1.0-f_{PGE}, obtained under stoichiometric conditions with different fractions of PGE (f_{PGE} from 0.10 to 0.50); △: systems EP-$q-0.30$, obtained by varying q in the presence of PGE ($f_{PGE} = 0.30$).

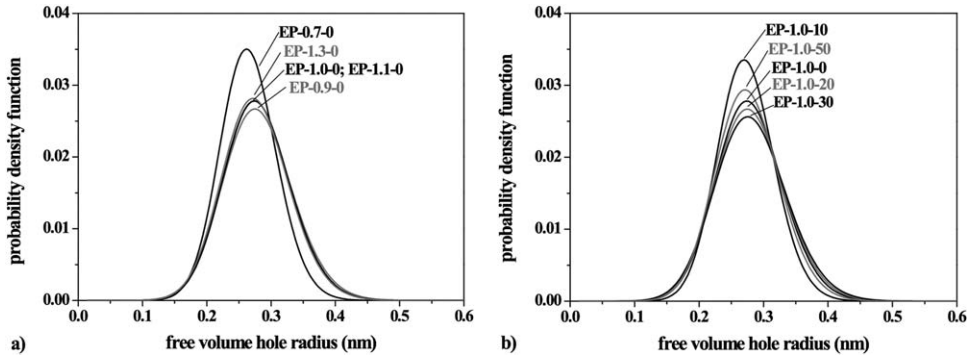

FIG. 3. Distribution of the probability density functions of the free volume holes radius for (a) the systems obtained by varying q in the absence of PGE and (b) systems obtained under stoichiometric conditions with different amounts of PGE.

of chemistry from that of free volume) and to the different methods of analysis for the annihilation spectra (distributed o-Ps component, chosen by us and Goyanes et al. [52] or discrete components [39, 53, 54]). However, the fact that variations of cross-link density were not mirrored by a systematic change in hole sizes was already shown for epoxy systems by Monnerie et al. [39].

Effect of Formulation on Glass Transition Temperature

DSC tests revealed that the optimized curing conditions assured full cross-linking on all the prepared resins, as evidenced by the absence of any exothermal signal in the first heating scan and by the very similar appearance of the first and second heating scan. The second scan typically provided a better defined glass transition region, where possible enthalpy relaxation effects are minimized thanks to the controlled cooling conditions. For this reason, the glass transition temperature was evaluated for all the systems on the second heating scan.

The values of T_g, measured as inflection point in the DSC second heating scan and as loss modulus peak temperature in the DMA traces, are reported in Table 2, with an overall good agreement among the values determined by the different techniques. In Fig. 4a, the values measured in DSC tests are represented as a function of q. As expected, the material composition has an important effect on the glass transition temperature. The value of T_g is seen to attain a maximum value for the systems obtained by mixing bifunctional epoxy resin and amine hardener with nearly stoichiometric composition. Changing the composition toward either a resin or a hardener excess leads to a reduction of the glass transition temperature, and a similar effect is promoted by introducing larger fractions of monofunctional epoxy resin. Both strategies may be considered convenient to promote a reduction in T_g, and in particular the addition of PGE, is seen to provide the more effective T_g reductions.

The dependence of the glass transition on the parameters of formulation is very similar to that found for the cross-link density. Figure 4b represents the glass transition temperature of the various systems as a function of the cross-link density, highlighting a common increasing trend for all the systems, in spite of their different macromolecular architectures, and evidencing that the α-transition temperature is governed by the network density. This finding may be interpreted in the light of literature models [55, 56], such as that proposed by Marzio [56], which postulates:

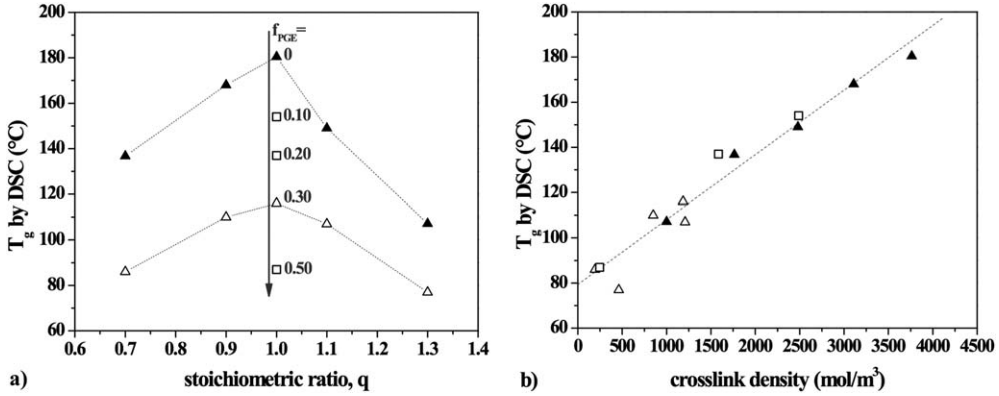

FIG. 4. Glass transition temperature evaluated through DSC analysis as a function of (a) the stoichiometric ratio and (b) the cross-link density (▲: systems EP-$q-0$, obtained by varying q in the absence of PGE; □: systems EP-1.0-f_{PGE}, obtained under stoichiometric conditions with different fractions of PGE (0.10; 0.20; 0.50); △: systems EP-$q-0.30$, obtained by varying q in the presence of PGE ($f_{PGE} = 0.30$).

DOI 10.1002/pen

TABLE 3. Results of the tensile tests at room temperature.

Material code	Modulus, E (MPa)	Stress at break, σ_b (MPa)	Strain at break, ε_b (%)
EP-0.7-0	2740 ± 70	71 ± 1	8.0 ± 0.8
EP-0.9-0	2489 ± 8	60 ± 20	6 ± 3
EP-1.0-0	2710 ± 150	42 ± 15	3 ± 2
EP-1.1-0	2790 ± 110	70 ± 9	5 ± 2
EP-1.3-0	3570 ± 110	82 ± 5	4.0 ± 0.7
EP-1.0-0.10	2894 ± 1	68 ± 6	5.7 ± 0.1
EP-1.0-0.20	3010 ± 80	63 ± 6	3.8 ± 0.8
EP-1.0-0.30	3300 ± 300	76 ± 2	5.1 ± 0.3
EP-1.0-0.50	3500 ± 300	64 ± 4	2.6 ± 0.1
EP-0.7-0.30	3300 ± 50	77 ± 3	4.9 ± 0.5
EP-0.9-0.30	3300 ± 100	81 ± 1	8.5 ± 1.4
EP-1.1-0.30	3320 ± 80	83.2 ± 0.5	4 ± 2
EP-1.3-0.30	3521 ± 25	72 ± 2	4.2 ± 0.5

$$T_g = \frac{T_{gl}}{1 - KFv} \tag{10}$$

where the value of T_g is seen to depend on cross-link density through the following material parameters: T_{gl} which represents the glass transition temperature of an hypothetical equivalent linear copolymer containing all the network difunctional units; F, a flex parameter representative of the chain stiffness, typically increasing with the content of aromatic groups; K, an universal constant, equal to ~2 for trifunctional cross-links when the cross-link density is expressed in chain concentration [16]. The curve of Fig. 4b highlights for all the resin a common trend and, thus, suggests very similar values of T_{gl} and F for all the formulations. The results may be justified on the basis of the similar flexibility of all the elastically active network chain segments composing the various network structures, due to the presence of stiff aromatic groups in their backbone. Consistently, in the work of Bellenger et al. [57], it is shown that for DGEBA/DDM systems prepared under various amine excesses, the theoretical values of T_{gl} and F are very slightly affected by the changes in the system formulation. Moreover, these theoretical values have seen to be in a generally good agreement with those determined experimentally from the data of Fig. 4b (for our systems T_{gl} is equal to about 356 K and F is equal to about 35 g/mol).

Effect of Formulation on the Small Deformation Behavior

The behavior of the various resins at small deformations was evaluated in uniaxial tensile tests and in dynamic-mechanical analysis, carried out on the bar-shaped specimens.

Tensile tests were performed at room temperature (i.e., within the glassy region for all the systems) up to specimen failure. Table 3 reports the tensile modulus, E, and the stress and strain at break (σ_b and ε_b, respectively) for the various materials.

The room temperature elastic modulus displays an evident dependence on material composition, with an overall variation between about 2.5 and 3.5 GPa. As represented in Fig. 5, the values of the glassy Young's modulus show a minimum value for the resin EP-0.9-0; a slight increase of modulus is found when both reducing q toward 0.7 and increasing q up to 1.1, whereas a significant modulus enhancement is found in case of a higher excess of resin (q = 1.3) or in the presence of PGE; finally, the variation of the stoichiometric ratio had limited influence on material stiffness in the presence of 30% of PGE, probably as a consequence of the already relatively high amount of this network modifier.

For what concerns their ultimate properties, all materials underwent brittle failure, presenting an abrupt drop of the stress *versus* strain curves at moderate levels of strain, with no evident sign of plasticity. The reference system EP-1.0-0 shows the lowest strength and is one of the systems with the lowest elongation at break, whereas each attempt at modifying the system formulation led to an increase in strength up to 100%, and suggests also an increase in the elongation at break, although the results on this variable are more scattered.

The tensile behavior seems thus to display the typical phenomenology related to antiplasticization. This is particularly evident in Fig. 6, where Young's modulus is seen to decrease as T_g

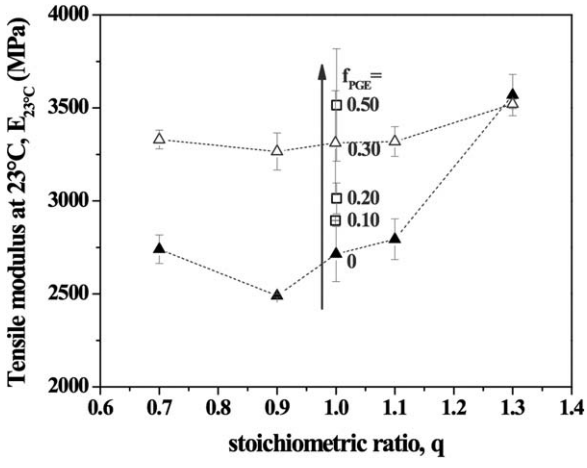

FIG. 5. Tensile modulus as a function of the stoichiometric ratio for the various materials (▲: systems EP-q−0, obtained by varying q in the absence of PGE; □: systems EP-1.0-f_{PGE}, obtained under stoichiometric condition with different fractions of PGE (0.10; 0.20; 0.50); △: systems EP-q−0.30, obtained by varying q in the presence of PGE (f_{PGE} = 0.30).

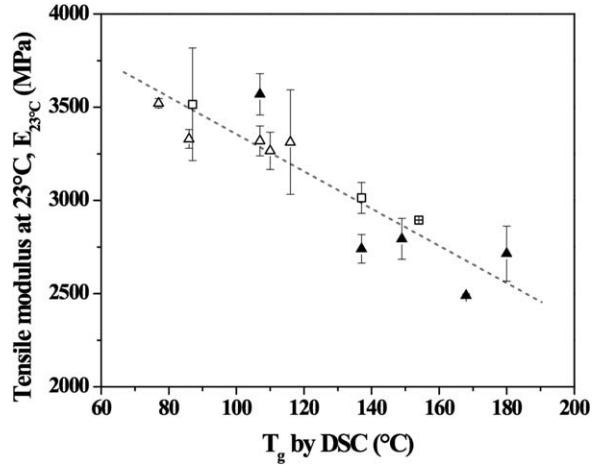

FIG. 6. Tensile modulus *versus* T_g for the various materials (▲: systems EP-q−0, obtained by varying q in the absence of PGE; □: systems EP-1.0-f_{PGE}, obtained under stoichiometric condition with different fractions of PGE (0.10; 0.20; 0.30; 0.50); △: systems EP-q−0.30, obtained by varying q in the presence of PGE (f_{PGE} = 0.30).

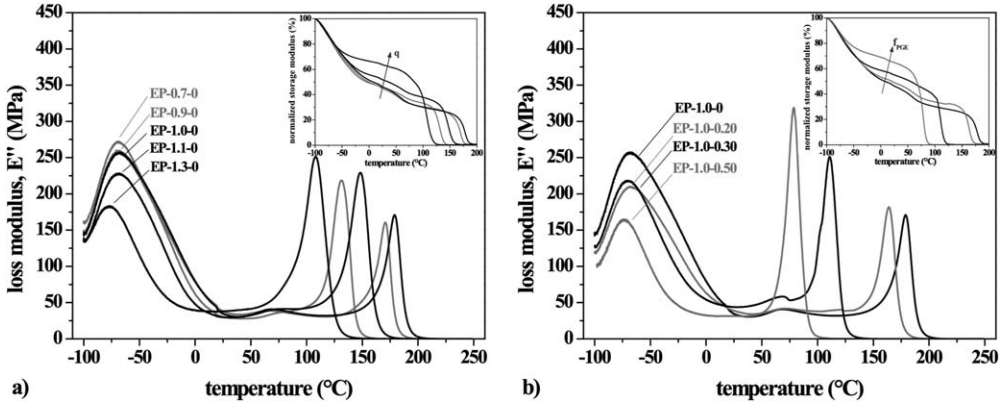

FIG. 7. Loss modulus traces for some of the systems investigated: (a) systems obtained by varying q in the absence of PGE and (b) systems obtained under stoichiometric conditions with different amounts of PGE. Insets: normalized storage modulus (see *Eq. 11*) as a function of temperature.

increases, as commonly reported also for other antiplasticized epoxy systems [24–26, 28, 58–61].

To better investigate this point, DMTA tests were carried out on a region including both primary and secondary relaxations. In fact, antiplasticization is usually ascribed to an inhibition of short range backbone movements (i.e., β-relaxations), due to strong intermolecular interactions [26] and/or to specific molecular architecture [61].

The effect of q and f_{PGE} on secondary relaxation is shown in Fig. 7a and b, respectively, where the loss modulus traces of the various materials are compared, so to directly highlight differences in the sub-T_{room} peaks; further, in the insets, the overall change in material stiffness with temperature is reported in terms of storage modulus value normalized to its value at the lowest temperature (i.e., -100°C), according to equation:

$$\text{normalized storage modulus}\,(\%) = \frac{E'(T)}{E'(-100^{\circ}\text{C})} \times 100 \qquad (11)$$

Three relaxation processes can be identified from the DMA loss modulus curves: (1) the primary relaxation process (α-transition), related to the glass transition, occurring at the highest temperature for each system and leading to a decrease of modulus from about 3 GPa to tens of MPa; (2) a secondary process (β-transition), mainly evidenced by a peak at about -65°C in the loss modulus traces, ascribed to the crankshaft rotation of hydroxypropylether units and involving a decrease of the storage modulus from about 6 to 3 GPa; and (3) a minor relaxation process taking place at about 60°C, which is evidenced as a peak in the E'' traces for most of the materials, while for some materials being overlapped by the α-transition peak (EP-1.0-0.5) or consisting in a shoulder in the low temperature part of the primary relaxation process (EP-1.3-0).

In particular, in Fig. 7a it is shown that by increasing the value of q the β-relaxation peak decreases in intensity and presents a narrower distribution on the temperature scale, especially for the networks obtained with an excess of epoxy. Similarly, in Fig. 7b, a higher PGE content is shown to promote a reduction of the β-transition peak intensity and width.

The inhibition of β-relaxation process may have an important effect on room temperature modulus, since, as discussed in various papers [22, 54, 55, 62, 63], the unrelaxed modulus of a material (i.e., its stiffness below any secondary sub-glassy relaxation) is determined by cohesive energy density, whereas the modulus value measured at room temperature depends on the extent of the relaxation allowed by the sub-T_{room} transitions. Thus a reduction of sub-T_{room} secondary relaxations may lead to a higher room temperature modulus. This is particularly evident from the inset of Fig. 7b, where it is shown that incorporating larger fraction of PGE leads to a narrowing of the β-relaxation at about -65°C and to a more and more limited modulus reduction on this temperature region. Similarly, for all the systems obtained in resin excess, the increase of q tends to limit the extent of the modulus drop. Only the systems obtained using a hardener excess present a modulus decrease at about -65°C comparable to that of the stoichiometric bicomponent systems.

Similar considerations hold for the tan δ traces, reported in Fig. 8, and in particular in the insets, where the part of the trace corresponding to the β-transition is magnified. The traces confirm that by increasing the value of q the intensity of the β-relaxation tan δ peak decreases, and for the systems prepared with an epoxy excess a significant and progressive narrowing of the peak distribution on the temperature scale is found (inset of Fig. 8a). A similar narrowing of the β-relaxation peak is shown for the highest PGE contents, in systems EP-1.0-0.30 and Ep-1.0-0.50 (Fig. 8b).

These results are particularly interesting because they describe the effects played by a specific resin formulation on the antiplasticization phenomenon. In particular, it may be found out that antiplasticizing effects are exerted mainly by resin excess and by the addition of PGE, whereas no appreciable effects are shown for amine excess. The antiplasticization effect can thus be primarily ascribed to the presence and relative amount of the dangling chains, increasing both as the excess of resin and as the PGE content increase. The different behavior found for the hardener excess is justified by the fact that different types of unreacted groups are expected in this case. Theoretically, these moieties may be represented by dangling aromatic amine chains and unreacted amine hydrogens, and the latter are more probable due to the higher reactivity of the primary amine hydrogen with the unreacted epoxy monomer compared to the secondary amine hydrogens [64]. In the case of a structure rich

 DOI 10.1002/pen

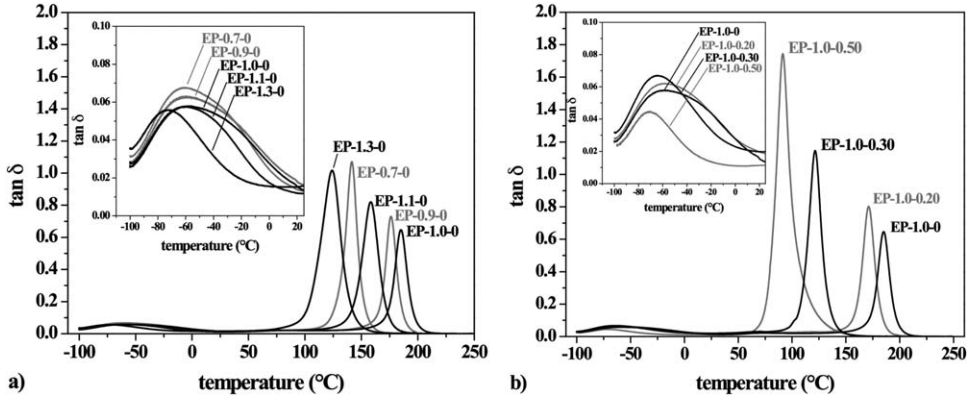

FIG. 8. Tan δ traces for some of the systems investigated: (a) systems obtained by varying q in the absence of PGE and (b) systems obtained under stoichiometric conditions with different amounts of PGE. Insets: magnification of the traces in the β-transition zone.

in unreacted hydrogens, the hindrance effect of dangling groups on β-relaxation may be considered negligible, and only the primary relaxation process is affected, due to a reduction of the cross-link density.

Effect of Formulation on Large Deformations Behavior

The large deformation behavior of the resins was investigated in uniaxial compression tests, since under these conditions the tendency to brittle failure is suppressed and the materials may be tested well above yielding. The results are reported as true compressive stress *vs*. true compressive strain in Fig. 9a and b.

All the investigated materials display a common behavior, consisting in an early initial linear trend, followed first by the approach of a stress peak, representative of the yield point, by a subsequent strain softening region, in which the stress drops until a minimum point, and finally by the strain hardening region, in which the stress progressively increases with the strain. Only the resin EP-1.0-0 presents a monotonous increase of stress with strain, with no evidence of a maximum yield point, nor of a strain softening process: for this system, the true stress progressively increases up to a saddle point (or to a narrow plateau) at a strain equal to about 0.19 to subsequently strain harden at higher strains. Further, EP-1.0-50 displayed fracture at the beginning of the strain hardening region, through localized cracking and transverse splitting of the cylinders.

The stress *vs*. strain correlation is strongly dependent on the system formulation. The main differences are related to the yield point, to the intensity of the stress drop after yielding and to the slope of the curve in the strain hardening region. More specifically, the yield stress generally increases with the PGE content and, in a less regular manner, as the q ratio increases; the stress drop in the softening region becomes more pronounced the more the q ratio departs from unity and the higher the PGE content; similar considerations hold for the slope of the curve in the strain hardening region.

To quantitatively describe all these effects, Table 4 provides the following parameters: yield stress and strain ($\sigma_{t,y}$ and $\varepsilon_{t,y}$, respectively), evaluated in correspondence of the stress peak maximum; plastic flow stress and strain ($\sigma_{t,f}$ and $\varepsilon_{t,f}$, respectively), evaluated in correspondence to the stress minimum, and the so-called yield drop ($\Delta\sigma_{t,f} = \sigma_{t,y} - \sigma_{t,f}$); the strain hardening modulus, G_{SH}, evaluated through *Eq. 8*. In the case of resin EP-1.0-0, where no evident maximum stress is displayed, the yield stress was arbitrarily reported as the stress at saddle point, and, in absence of a proper strain softening point, no flow stress was

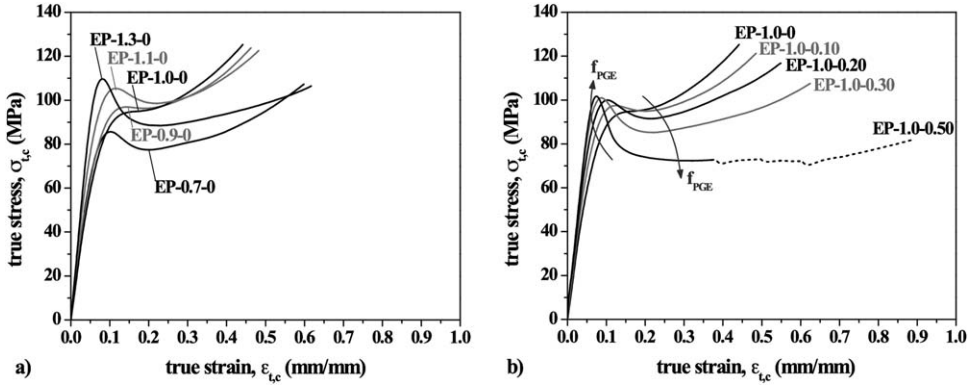

FIG. 9. True compressive stress *vs*. true compressive strain curves for (a) systems obtained by varying q in the absence of PGE and (b) systems obtained under stoichiometric conditions with different amounts of PGE; the last portion of the curve for system EP-1.0-0.5 is represented by a dashed line, since the specimen underwent localized failure.

TABLE 4. Results of the compression tests at large strains ($\sigma_{t,y}$: true yield stress; $\varepsilon_{t,y}$: true yield strain; $\sigma_{t,f}$: true flow stress; $\varepsilon_{t,f}$: true flow strain; $\Delta\sigma_{t,f}$: yield drop; G_{SH}: strain hardening modulus).

Material code	$\sigma_{t,y}$ (MPa)	$\varepsilon_{t,y}$ (mm/mm)	$\sigma_{t,f}$ (MPa)	$\varepsilon_{t,f}$ (mm/mm)	$\Delta\sigma_{t,f}$ (MPa)	G_{SH} (MPa)
EP-0.7-0	85 ± 1	0.101 ± 0.003	77.1 ± 1.2	0.206 ± 0.007	8.4 ± 0.3	50.2 ± 1.5
EP-0.9-0	97.0 ± 0.3	0.144 ± 0.004	96.1 ± 0.4	0.194 ± 0.007	0.82 ± 0.17	67.4 ± 1.0
EP-1.0-0	94.5 ± 0.5[a]	0.165 ± 0.006[a]	–[b]	–[b]	0[b]	69.0 ± 2.0
EP-1.1-0	106 ± 1	0.1140 ± 0.0007	99.4 ± 1.5	0.209 ± 0.006	6.2 ± 0.6	55.0 ± 1.7
EP-1.3-0	109.1 ± 0.5	0.10805 ± 0.0006	88.2 ± 0.3	0.214 ± 0.015	20.8 ± 0.4	26.8 ± 2.7
EP-1.0-0.10	98 ± 1	0.1259 ± 0.0004	94.3 ± 0.9	0.200 ± 0.009	2.49 ± 0.08	57.5 ± 2.2
EP-1.0-0.20	99.6 ± 0.5	0.100 ± 0.0015	90.8 ± 0.6	0.211 ± 0.009	8.7 ± 0.2	44.2 ± 1.9
EP-1.0-0.30	100.3 ± 0.8	0.0866 ± 0.0004	84.9 ± 0.7	0.22 ± 0.01	15.4 ± 0.3	36.4 ± 1.2
EP-1.0-0.50	102.9 ± 1.3	0.0742 ± 0.0008	72.24 ± 0.16	0.28 ± 0.03	30.7 ± 0.8	–[c]
EP-0.7-0.30	105.9 ± 0.3	0.080 ± 0.005	75.6 ± 0.4	0.32 ± 0.03	30.31 ± 0.19	9.9 ± 0.7
EP-0.9-0.30	105.2 ± 0.5	0.093 ± 0.003	86.0 ± 0.9	0.226 ± 0.002	19 ± 1	25 ± 5
EP-1.1-0.30	111.0 ± 1.1	0.0890 ± 0.0009	88.9 ± 1.3	0.26 ± 0.04	22.1 ± 0.7	30 ± 5
EP-1.3-0.30	113.6 ± 0.5	0.079 ± 0.004	77.6 ± 0.9	0.29 ± 0.018	36 ± 1	17.7 ± 1.9

[a]Stress/strain at the saddle point of the stress *versus* strain curve.
[b]No flow stress or yield drop could be determined.
[c]No strain hardening modulus was determined since the materials underwent local damaging.

provided and the yield drop was taken as zero. In the case of resin EP-1.0-0.50 no strain hardening modulus was determined due to specimen failure on the corresponding region.

The yield stress presents an overall variation from about 85 to 114 MPa, and it is evidently enhanced by the introduction of PGE and by the adoption of some off-stoichiometric formulations. The yield strain, which is located between 0.07 and 0.17, is higher for the systems near the stoichiometric composition and incorporating less PGE.

The behavior at yield is suggested to reflect closely the antiplasticization phenomenology, similarly to what observed for the room temperature tensile modulus (see Fig. 6). To highlight a certain analogy with this latter mechanical property, in Fig. 10 the yield stress is represented as a function of the glass transition temperature.

The similar dependence of yield stress and tensile modulus on formulation was the argument employed by Rana et al. [30] to explain the occurrence of antiplasticization in epoxy-amine systems, ascribing the effect to the reduction of the cooperative β-motions, which determines a more cohesive material and, consequently, a larger resistance to plastic deformation. It is noteworthy to remark that, for our systems, the higher yield stress is usually displayed by less cross-linked systems: since a lower cross-link density is expected to enhance the overall network chain mobility through an enhancement of α-type relaxation motions, it becomes evident that the increase in yield stress is mainly determined by local hindrance of β-relaxation, due to dangling chains. Furthermore, in support of this idea it is worth noting also that tests were carried out far from T_g, that is, under a condition for which the network segments possess only limited large-scale mobility. Finally, the idea of a local mobility hindrance governing this strain regime could be also confirmed by the occurrence of yielding at lower strains for the systems incorporating larger amounts of dangling chains (i.e., the off-stoichiometry systems, and the systems richer in PGE).

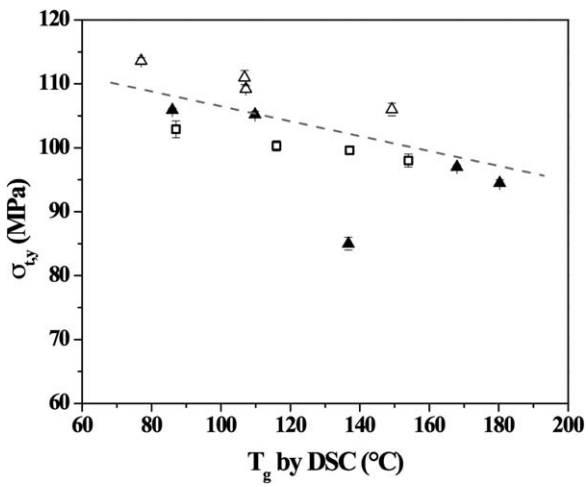

FIG. 10. True yield stress, $\sigma_{t,y}$, *versus* T_g for the various materials (▲: systems EP-q−0, obtained by varying q in the absence of PGE; □: systems EP-1.0-f_{PGE}, obtained under stoichiometric condition with different fractions of PGE (0.10; 0.20; 0.30; 0.50); △: systems EP-q−0.30, obtained by varying q in the presence of PGE (f_{PGE} = 0.30).

By contrast, the postyield softening and hardening behavior seems to be mainly influenced by the cross-link density, and for the interpretation of the results it is important to remark that at these relatively high levels of strain, the deformation mechanisms are those connected to a long range mutual sliding of the network chains.

The flow stress and the strain softening amplitude are usually strongly related to the cross-link density, since the presence of a tight network structure tends to stabilize the softening behavior and to reduce the yield drop [27]. Our results clearly suggest that any deviations from the high cross-link density of the stoichiometric binary system promotes a higher compliance in the strain softening region, that is, a reduction of flow stress and an increase in the strain softening amplitude. The effects of the cross-link density on flow stress, $\sigma_{t,f}$, and on the strain softening amplitude, $\Delta\sigma_{t,f}$, are represented in Fig. 11a and b, respectively. The values of flow stress are seen to increase with the cross-link density, presenting for all the materials a common increasing trend, independently from the resin formulation, and approaching a sort of steady state at about of 95 MPa for the most cross-linked systems. Concurrently, more important strain

 DOI 10.1002/pen

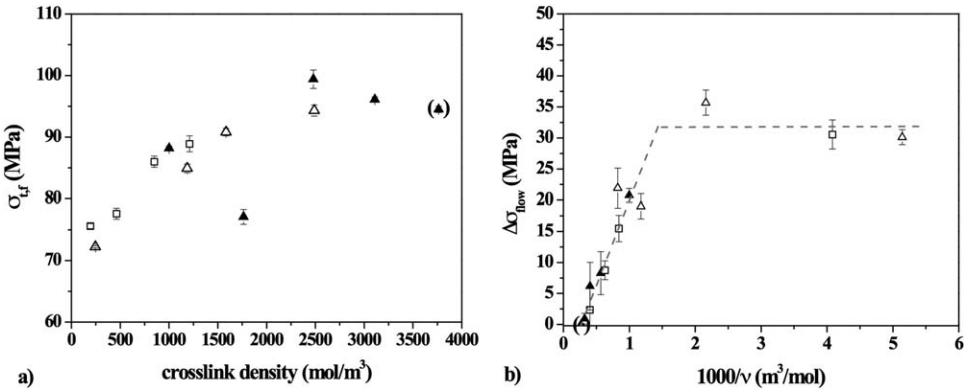

FIG. 11. (a) Plastic flow stress, $\sigma_{t,f}$ as a function of the cross-link density, and (b) strain softening amplitude, $\Delta\sigma_{t,f}$ as a function of the inverse of the cross-link density for the various materials (▲: systems EP-$q-0$, obtained by varying q in the absence of PGE; □: systems EP-1.0-f_{PGE}, obtained under stoichiometric condition with different fractions of PGE (0.10; 0.20; 0.50); △: systems EP-$q-0.30$, obtained by varying q in the presence of PGE ($f_{PGE} = 0.30$). Values between brackets represent the system EP-1.0-0, for which no minimum point is found: $\sigma_{t,f}$ is taken as $\sigma_{t,y}$ and $\Delta\sigma_{t,f}$ as zero.

softening amplitudes are shown for less cross-linked systems; in particular, for a network density above 500 mol/m^3, the entity of the drop decreases with ν, as a consequence of the stabilizing effect of the network; by contrast, for lower ν values the entity of the drop becomes practically constant and independent from network density, since for a very loose network the ability to flow is mainly dictated by the ability of the network chains to slip.

For what concerns the strain hardening behavior, the slope of the stress *versus* strain curve in this region was evaluated for the various materials and defined as strain hardening modulus, G_{SH}, according to *Eq. 8*. The modulus was determined after having represented the compression test outputs as $\sigma_{t,c}$ *versus* $-(\lambda^2-1/\lambda)$, since such a representation allows to evidence linear correlation between the two variables, as shown by Haward for amorphous glassy polymers at large deformations [65]. Since a proper linearization over the whole strain hardening region was not found for our systems, the values of G_{SH} were evaluated as the slope on the last 20% of strain before the end of the test.

The results are reported in Fig. 12, where the strain hardening modulus is represented as a function of the cross-link density, evidencing for all resins a unique dependence of the strain hardening modulus on ν. Such a ruling influence of the cross-link density, discussed in other works for physically entangled and cross-linked plastics [27, 31, 66], may be ascribed to the specific deformation mechanism taking place in the strain hardening regime, which involves the progressive stretching of the network segments in the polymeric matrix.

As concluding remarks, from the above discussed results, we may observe that dangling chains and network density may have different effects depending on temperature and strain scale. At very low temperatures (i.e., below secondary transitions) the mechanical behavior is dominated by cohesive forces; as temperature increases above the secondary transition region, the increase in material compliance is controlled by the ability of dangling chains to suppress local chain mobility; only above the glass transition temperature the obstacle to chain motion is provided by netpoints and the behavior is governed by the cross-link density. At room temperature, which for our resins is above secondary relaxation and below the primary one, the local chain mobility suppression exerted by dangling chains affects the mechanical response as long as the strain level is small (early elastic response and onset of the yielding process): in fact, since at these levels of strain, the deformation mechanisms do not involve important mutual sliding of the network chains, the contribution of cross-link density is of minor importance. When moving along the strain scale toward higher strain, mutual slipping of the network chain is activated, the hindering effect of pending groups becomes less effective above yield point, and the effect of antiplasticization becomes negligible with respect to that of the network. Consequently, increasing network density leads to a stiffer response in the large deformation range, as testified by: (1) the increasing value of stress required to activate chain flow; (2) the reduction, until final suppression, of the

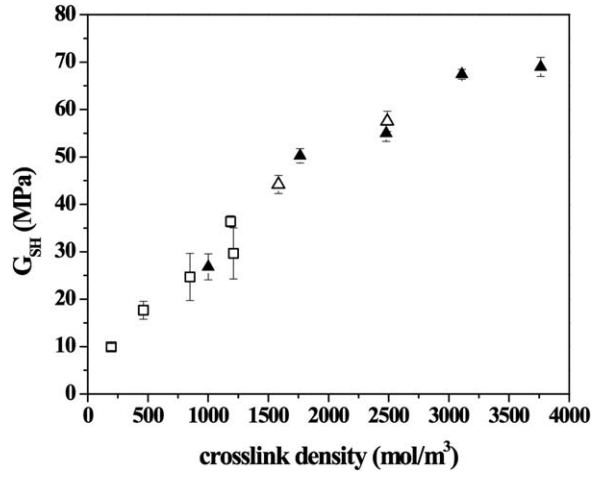

FIG. 12. Strain hardening modulus as a function of the cross-link density for the various materials (▲: systems EP-$q-0$, obtained by varying q in the absence of PGE; □: systems EP-1.0-f_{PGE}, obtained under stoichiometric condition with different fractions of PGE (0.10; 0.20; 0.50); △: systems EP-$q-0.30$, obtained by varying q in the presence of PGE ($f_{PGE} = 0.30$).

strain softening; and (3) the increase in strain hardening modulus.

CONCLUSIONS

In this work a series of structurally related epoxies were prepared with the main aim to interpret, in the light of structural considerations, their mechanical behavior both at small and large (yield and postyield) strain regimes.

The resins were obtained as properly designed mixtures of a diepoxide resin, a monoepoxide resin, and an aromatic diamine hardener. This approach allowed to tune the resins macromolecular architecture in terms of cross-link density and of the type and amount of dangling groups. The change in the material formulation is demonstrated to greatly affect both thermal and mechanical response of the systems.

The effects on thermal properties regard mainly the characteristic temperature and extent of the relaxation processes. It is shown that the material network density completely controls and largely alters the temperature of the primary relaxation process (i.e., T_g), whereas the presence of dangling chains suppresses the β-type relaxation motions. More precisely, by increasing the number of epoxy dangling residues, an effective restriction of the β-type relaxation capabilities is found, whereas in case of amine excess only a slight variation, if any, of the secondary relaxation process is found.

The suppression of the β-type relaxation motions was interpreted as the main cause of the stiffening effect measured on the room temperature tensile modulus and compressive yield stress for less cross-linked systems. The occurrence of an increase in stiffness and yield strength, together with a simultaneous reduction of T_g, allowed to describe the material behavior at the small strain and up to yield as due to an antiplasticization effect. Furthermore, the absence of significant changes in the free volume, as revealed by positron annihilation lifetime spectroscopy, suggests that free volume would play a minor role compared to secondary transitions to explain the observed antiplasticization effects. When moving to higher levels of strains, the role of the network density becomes more important, and it was shown that a higher cross-link density promotes larger flow stress and higher strain hardening modulus, while it reduces, to complete elimination, the extent of the strain softening region.

ACKNOWLEDGEMENT

The authors gratefully acknowledge Ms Isabella Peroni and Ms Gloria Spagnoli for their kind support in the materials preparation.

REFERENCES

1. J.R.M. D'Almeida and S.N. Monteiro, *Polym. Test.*, **15**, 329 (1996).
2. F. Fernandez-Nograro, A. Valea, R. Llano-Ponte, and I. Mondragon, *Eur. Polym. J.*, **32**, 257 (1996).
3. G.R. Palmese and R.L. McCullough, *J. Appl. Polym. Sci.*, **46**, 1863 (1992).
4. C.L. Sherman, R.C. Zeigler, N.E. Verghese, and M.J. Marks, *Polymer*, **49**, 1164 (2008).
5. F. Bignotti, S. Pandini, F. Baldi, and R. De Santis, *Polym. Compos.*, **32**, 1034 (2011).
6. S. Pandini, F. Baldi, R. De Santis, and F. Bignotti, *Polym. Compos.*, **32**, 1461 (2011).
7. S. Pandini, F. Bignotti, F. Baldi, and S. Passera, *J. Intell. Mater. Syst. Struct.*, **24**, 1583 (2013).
8. S. Pandini, F. Bignotti, F. Baldi, and L. Sartore, *AIP Conf. Proc.*, **1736**, 020173 (2016).
9. M.R. Vanlandingham, R.F. Eduljee, and J.W. Jr. Gillespie, *J. Appl. Polym. Sci.*, **71**, 699 (1999).
10. F. Meyer, G. Sanz, A. Eceiza, I. Mondragon, and J. Mijović, *J. Polym.*, **36**, 1407 (1995).
11. K.J. Calzia and A.J. Lesser, *J. Mater. Sci.*, **42**, 5229 (2007).
12. E. Crawford and A.J. Lesser, *J. Polym. Sci. B: Polym. Phys.*, **36**, 1371 (1998).
13. N. Droger, O. Primel, and J.L. Halary, *J. Appl. Polym. Sci.*, **107**, 455 (2008).
14. A.E. Mayr, W.D. Cook, and G.H. Edward, *Polymer*, **39**, 3719 (1998).
15. E. Urbaczewski-Espuche, J. Galy, J. Gerard, J.P. Pascault, and H. Sauterau, *Polym. Eng. Sci.*, **31**, 1572 (1991).
16. J.P. Pascault, H. Sautereau, J. Verdu, and R.J.J. Williams, *Thermosetting Polymers*, Marcel Dekker, New York (2002).
17. G. Levita, S. De Petris, A. Marchetti, and A. Lazzeri, *J. Mater. Sci.*, **26**, 2348 (1991).
18. T.D. Chang and J.O. Brittain, *Polym. Eng. Sci.*, **22**, 1228 (1982).
19. F.A. Pfaff, *J. Coat. Technol. Res.*, **4**, 151 (2007).
20. J.R.M. D'Almeida and S.N. Monteiro, *J. Mater. Sci. Lett.*, **15**, 955 (1996).
21. J.R.M. D'Almeida and S.N. Monteiro, *Adv. Perform. Mater.*, **4**, 285 (1997).
22. R.P. Chartoff, J.D. Menczel, and S.H. Dillman, *Thermal Analysis of Polymers, Fundamentals and Applications*, John Wiley & Sons, Inc., Hoboken, NJ (2009).
23. J.T.A. Kierkels, C.L. Dona, T.A. Tervoort, and L.E. Govaert, *J. Polym. Sci. B: Polym. Phys.*, **46**, 134 (2008).
24. J. Daly, A. Britten, and A. Garton, *J. Appl. Polym. Sci.*, **29**, 1403 (1984).
25. S. Grishchuk, L. Sorochynska, O.C. Vorster, and J. Karger-Kocsis, *J. Appl. Polym. Sci.*, **127**, 5082 (2012).
26. S. Grishchuk, Z. Mbhele, S. Schmitt, and J. Karger-Kocsis, *eXPRESS Polym. Lett.*, **5**, 273 (2011).
27. H.G.H. Van Melick, L.E. Govaert, and H.E.H. Meijer, *Polymer*, **44**, 2493 (2003).
28. A.S. Zerda and A.J. Lesser, *Polym. Eng. Sci.*, **44**, 2125 (2004).
29. A.J. Lesser and R.S. Kody, *J. Polym. Sci. Polym. Phys. Ed.*, **35**, 1611 (1997).
30. D. Rana, V. Sauvant, and J.L. Halary, *J. Mater. Sci.*, **37**, 5267 (2002).
31. K.J. Calzia, A. Forcum, and A.J. Lesser, *J. Appl. Polym. Sci.*, **102**, 4606 (2006).
32. Y. Maeda and D.R. Paul, *J. Polym Sci. B: Polym. Phys.*, **25**, 1005 (1987).
33. G. Dlubek, F. Redmanm, and R. Krause-Rehberg, *J. Appl. Polym. Sci.*, **84**, 244 (2002).
34. J. Ubbink, *Adv. Drug Deliv. Rev.*, **100**, 10 (2016).
35. Y.C. Jean, J.D. Van Horn, W.S. Hung, and K.R. Lee, *Macromolecules*, **46**, 7133 (2013).

 DOI 10.1002/pen

36. K. Jeffrey and R.A. Pethrick, *Eur. Polym. J.*, **30**, 153 (1994).
37. C. Li and A. Strachan, *Polymer*, **97**, 456 (2016).
38. S. Goyanes, G. Rubiolo, A. Marzocca, W. Salgueiro, A. Somoza, G. Consolati, and I. Mondragon, *Polymer*, **44**, 3193 (2003).
39. L. Yang, H.A. Hristov, A.F. Yee, D.W. Gidley, D. Bauchiere, J.L. Halary, and L. Monnerie, *Polymer*, **36**, 3997 (1995).
40. G. Dlubek, E.M. Hassan, R. Krause-Rehberg, and J. Pionteck, *Phys. Rev. E*, **73**, 031803 (2006).
41. F.X. Perrin, M.H. Nguyen, and J.L. Vernet, *Eur. Polym. J.*, **45**, 1524 (2009).
42. G. Dlubek, *Polymer Physics from Suspensions to Nanocomposites and Beyond*, John Wiley & Sons, Singapore (2010).
43. L.R.G. Treloar, *The Physics of Rubber Elasticity*, Clarendon Press, Oxford, UK (1975).
44. I.K. MacKenzie and J. Fabian, *Nuovo Cimento*, **48B**, 162 (1970).
45. J. Kansy, *Nucl. Instrum. Methods Phys. Res. A*, **374**, 235 (1996).
46. B.A. Rozenberg, *Adv. Polym. Sci.*, **75**, 113 (1986).
47. Y.C. Jean, *Positron Spectroscopy of Solids*, IOS Press, Amsterdam (1995).
48. S.J. Tao, *J. Chem. Phys.*, **56**, 5499 (1972).
49. M. Eldrup, D. Lightbody, and J.N. Sherwood, *J. Chem. Phys.*, **63**, 51 (1981).
50. H. Nakanishi, Y.Y. Wang, Y.C. Jean, *Positron Annihilation Studies of Fluids*, *World* Scientific, Singapore (1988).
51. G. Consolati, *J. Chem. Phys.*, **117**, 7279 (2002).
52. S. Goyanes, W. Salgueiro, A. Somoza, J.A. Ramos, and I. Mondragon, *Polymer*, **45**, 6691 (2004).
53. K. Frank and J. Wiggins, *J. Appl. Polym. Sci.*, **130**, 264 (2013).
54. K. Frank, C. Childers, D. Dutta, D. Gidley, M. Jackson, S. Ward, R. Maskell, and J. Wiggins, *Polymer*, **54**, 403 (2013).
55. J.H. Gibbs and E.A.D. Marzio, *J. Chem. Phys.*, **28**, 373 (1958).
56. E.A.D. Marzio, *J Res Natl Bur Stand Sec. A*, **68**, 611 (1964).
57. V. Bellenger, W. Dhaoui, J. Verdu, J. Galy, Y.G. Won, and J.P. Pascault, *Polymer*, **30**, 2013 (1989).
58. J.L. Halary, *High Perform. Polym.*, **12**, 141 (2000).
59. S. Grishchuk, S. Schmitt, O.C. Vorster, and J. Karger-Kocsis, *J. Appl. Polym. Sci.*, **124**, 2824 (2012).
60. A. Pierre, O. Sindt, N. Thorne, J. Perez, and J.F. Gerard, *Macromol. Symp.*, **147**, 103 (1999).
61. T.-M. Don, J.P. Bell, and M. Narkis, *Polym. Eng. Sci.*, **36**, 2601 (1996).
62. S.A. Pellice, D.P. Fasce, and R.J.J. Williams, *Polym. Sci. B: Polym. Phys.*, **41**, 1451 (2003).
63. N. Kinjo and T. Nakagawa, *Polym. J.*, **4**, 143 (1973).
64. L. Matějka, *Macromolecules*, **33**, 3611 (2000).
65. M.C. Boyce and R.N. Haward, *The Physics of Glassy Polymers*, Chapman & Hall, London (1997).
66. L.E. Govaert and T.A. Tervoort, *J. Polym. Sci. B: Polym. Phys.*, **42**, 2041 (2004).